Thin Solid Films 757 (2022) 139392

Contents lists available at ScienceDirect

Thin Solid Films

journal homepage: www.elsevier.com/locate/tsf

Surfaces, Interfaces and Colloidal Behaviour

Effects of thermal vacuum nitridation of Si(100) surface via NH_3 exposure

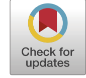

Masoud Ebrahimzadeh [a], Juha-Pekka Lehtiö [a], Marko Punkkinen [a], Risto Punkkinen [b], Mikko Miettinen [a], Zahra Sadat Jahanshah Rad [a], Mikhail Kuzmin [a], Pekka Laukkanen [a,*], Kalevi Kokko [a]

[a] Department of Physics and Astronomy, University of Turku, FI-20014 Turku, Finland
[b] Department of Computing, University of Turku, FI-20014 Turku, Finland

ARTICLE INFO

Keywords:
Dielectric film
Ammonia nitridation
Silicon passivation
Interface defects

ABSTRACT

Low temperature treatments to control the Si-interface properties become more and more relevant to the broad Si-based electronics and photonics technology when the back-end-of-line processing is developed and the integration of hybrid materials on the Si platform increases. In this work we have investigated effects of NH_3 nitridation of three different Si surfaces in ultrahigh-vacuum (UHV) chamber at 400 $^{\circ}C$: (i) nitridation of well-defined Si(100) (2 × 1)+(1 × 2) cleaned by the high-temperature flash heating, (ii) nitridation of the Radio Corporation of America (RCA)-cleaned H-terminated Si(100) with the final HF dip, and (iii) nitridation of the RCA-treated (without the final HF dip) Si(100) which includes so-called wet-chemical oxide of SiO_2. X-ray photoelectron spectroscopy (XPS) and scanning tunneling microscopy/spectroscopy measurements show that nitrogen incorporates into subsurface layers of clean Si and into the SiO_2 chemical-oxide layer, when the materials are exposed to NH_3 background in UHV chamber without a plasma source at 400 $^{\circ}C$ or even at room temperature. XPS results indicate that the nitridation does not remove oxygen from the SiO_2 chemical oxide. The nitridation of SiO_2 is also found to increase the density of electron levels at 3 to 4 eV above the Fermi level. Electrical measurements of atomic-layer deposited HfO_2/Si(100) capacitors with and without the nitridation support that the method has potential to decrease amount of interface defects and to control interface properties.

1. Introduction

Along with scaling down the size of various Si-based devices to increase the integration density and power efficiency, the insulator/Si junctions (or interfaces) that are a critical part of transistors, solar cells and sensors for example, have been intensively investigated and developed for several decades [e.g. 1–15]. Although understanding and processing of the Si-interface passivation (i.e. decreasing density of interface defects and their effects) have been refined to the top, requirements for low temperature (LT) processing of device structures have evoked different challenges also in the area of silicon technology [8–10]. LT treatment methods are needed for instance in the back-end-of-line processing of devices, where the temperature is often limited to 450 $^{\circ}C$, and for integrating complementary device materials on the established Si-wafer platform without degrading the material properties at elevated temperatures. The so-called thermal budget depends on the Si device type and the integrated material system. Promising device results have been obtained even with the 150 $^{\circ}C$ (or lower) passivation methods [10].

Various dielectric films have been investigated in the silicon technology; for example, SiO_2, Si_3N_4, Al_2O_3, HfO_2, ZrO_2, Gd_2O_3, NiO [1,2, 11-17]. These insulator-Si junctions still contain an interfacial SiO_2 layer because it is impossible to avoid the Si oxidation during the junction manufacturing, and because the Si oxidation is an energetically favored process [1,2]. Due to structural and electronic differences between oxide layers and semiconductor crystals, the interfaces often include high densities of point defects (e.g. vacancies and impurities) which further cause electronic defect levels in the Si band gap area. Because of the defect levels, the lifetime and energy efficiency of various current devices decrease.

Exposing Si surfaces to nitrogen-containing gas has been studied as a method to passivate the defect levels at the insulator/semiconductor junctions [18–25]. Silicon-nitrogen interactions have been studied even on atomic scale [e.g. 20-22], and a proper nitrogen incorporation has been found to provide a crystalline N-containing films at Si. Various techniques such as remote plasma nitridation, thermal nitridation with

* Corresponding author at: Department of Physics and Astronomy, University of Turku: Turun Yliopisto, Vesilinnantie 5, 20014 Turku, FI-20014 Turku, Finland.
E-mail addresses: masoud.m.ebrahimzadeh@utu.fi (M. Ebrahimzadeh), pekka.laukkanen@utu.fi (P. Laukkanen).

https://doi.org/10.1016/j.tsf.2022.139392
Received 29 December 2021; Received in revised form 27 June 2022; Accepted 12 July 2022
Available online 14 July 2022
0040-6090/© 2022 The Author(s). Published by Elsevier B.V. This is an open access article under the CC BY license (http://creativecommons.org/licenses/by/4.0/).

either NH_3 or N_2 have been found to decrease the defect density and the leakage current through the oxide film [18,23]. The N incorporation into the Si interfaces is as an important phenomenon not only for the transistor and memory technologies but also for photovoltaics and other photonics devices via integrating SiN_x or SiO_xN_y films with device structures [26–32]. Regarding industrial demands for processing various Si-based hybrid materials and devices, the LT process is becoming of high importance [8-10,18,27,28].

In this work, the formation of SiN_x and SiO_xN_y films has been investigated using thermal NH_3 nitridation of Si(100) and of oxidized Si (100) surfaces in the ultrahigh vacuum (UHV) chamber at 400 °C or below by controlling NH_3 partial pressure and exposure. It is worth noting that the nitridations have been done in this work without a plasma source. Although the plasma source methods have clear benefits, for example, to enhance nitrogen incorporation at low substrate temperatures, the plasma is also known to cause material defects [e.g. 29-32]. Therefore, we have in this work focused on the nitridations without the plasma. For electrical characterization of the interfaces, HfO_2 films have been deposited by atomic layer deposition (ALD) to prepare HfO_2/SiO_xN_y/Si(100) junctions with the nitridation and also reference samples of HfO_2/SiO_x/Si(100) without the nitridation. Electrical properties of the interfaces have been investigated by capacitance voltage (C-V) and leakage current (I-V) measurements of capacitors. Properties of the NH_3-treated surfaces have been also studied by x-ray photoelectron spectroscopy (XPS), low energy electron diffraction (LEED), and scanning tunneling microscopy/spectroscopy (STM/STS). The outline of this article is following: We have first investigated the nitridation of a well-ordered substrate surface of Si(100)(2 × 1)+(1 × 2), which is obtained by the flash heating up to 1200 °C in UHV. The knowledge obtained from such a well-defined model system is then transferred to the studies of industrially potential wet-chemically cleaned Si surfaces, in order to perform a whole interface passivation procedure below 450 °C. Two different wet-chemically treated Si surfaces (with the Radio Corporation of America, RCA recipe) have been used in the nitridation studies: the RCA-cleaned hydrogen-terminated Si surface and the RCA-prepared oxide-terminated Si surfaces.

2. Experimental Section

Fig. 1 summarizes the sample preparation. Pieces of 6 × 12 mm were cut from n-type Si(100) wafer (phosphorus-doped) with a resistivity of 3-9 Ω cm. To clean the Si surfaces from oxides and contaminants, we used two different methods: (i) high temperature (1200 °C) flash heating in UHV system and (ii) RCA chemical cleaning recipe with the following steps: (a) C_3H_6O 3 min at RT + nitrogen drying; (b) CH_3OH 3 min at RT + nitrogen drying; (c) C_3H_8O 3 min at RT + nitrogen drying; (d) H_2SO_4:H_2O_2 (3:1), 15 min at 80 °C + deionized water rinsing + nitrogen drying; (e) H_2O:NH_4OH:H_2O_2 (5:1:1), 15 min at 80 °C + deionized water rinsing + nitrogen drying; (f) H_2O:HCl:H_2O_2 (6:1:1), 15 min at 80 °C + deionized water rinsing + nitrogen drying.

The RCA procedure was ended up with or without HF (5%) solution dip for 5-10 s. The HF dip is known to remove oxides and provide a hydrogen terminated surface, which is expected to decrease the regrowth of native oxides during a short air exposure. On the other hand, the samples without the HF dip included a thin SiO_2 oxide film, called often the wet-chemical oxide (or SC-2 oxide).

After RCA, the samples were transferred into the UHV multi-chamber system within 2-10 min through the air. In the UHV system, both sample types: the H-terminated and oxidized Si surfaces were heated at 400 °C for 30 min after RCA (exceptions are mentioned in text). Nitridation of the Si surfaces cleaned by the different methods was performed by keeping the Si substrate in NH_3 gas for 30 min or 60 min either at two different temperatures: room temperature (RT) or at 400 °C. NH_3 partial pressure was approximately 5×10^{-3} Pa, whereas the base pressure of the process chamber was 1×10^{-6} Pa, and no plasma source was used. Furthermore, NH_3 purity was 99.9999%, and a total nitridation dose was either 18.3×10^3 L (30 min) or 36.7×10^3 L (60 min).

In situ LEED, STM/STS, and non-monochromatized XPS measurements were done to study surface properties of the samples before and after the nitridation. Omicron Scala instrument was used in constant current mode for STM measurement. The grid mode was used to measure the current-voltage curves in STS, which were averaged over chosen surface areas and differentiated afterwards. Also, another XPS instrument with monochromator (Al-Kα) was used in *ex situ* manner to measure the Si surface after nitridation and air transfer.

ALD equipment was used to grow HfO_2 films on top of some samples. All these samples were loaded into the ALD system via air. The precursors are tetrakis (dimethylamido) hafnium and H_2O for HfO_2 film. The film thickness was 15 nm as measured by ellipsometry. Metal-oxide-semiconductor capacitors were fabricated to measure C-V and I-V curves. Au/Cr or Ag/Cr metal contacts (circular pads with 200 µm diameter) were deposited on HfO_2/n-Si(100) by sputtering through a shadow mask. Finally, the post metallization heating was performed at 400 °C for 20 min in the UHV system. C-V and I-V measurements were

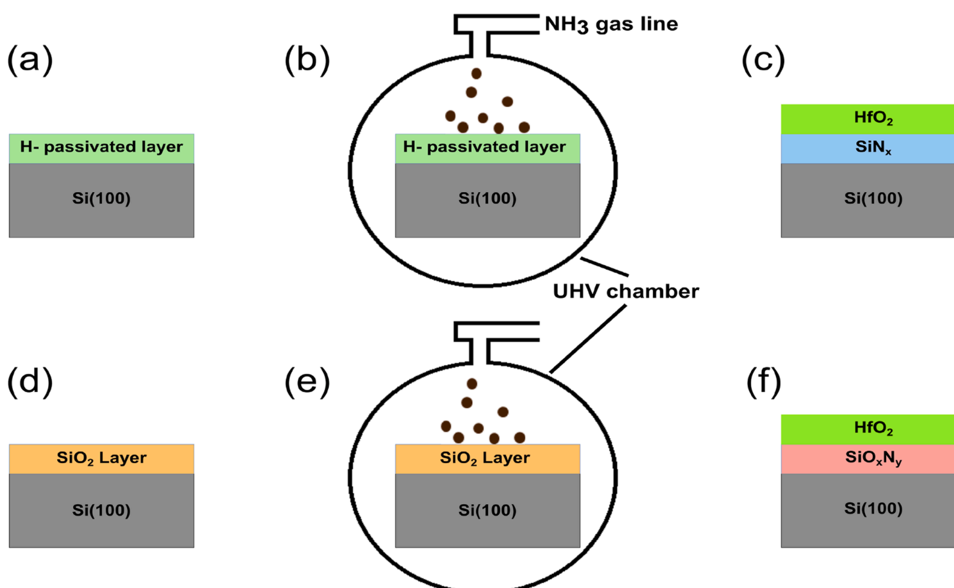

Fig. 1. Schematic of HfO_2/SiN_x/Si(100) samples treated with the RCA method. **(a)** RCA cleaned surface with HF dipping. HF dip causes hydrogen passivated surface. **(b)** NH_3 treatment (5×10^{-3} Pa, 400 °C) in the UHV chamber. **(c)** Oxide layer (HfO_2 ~15 nm thick) deposition by ALD, and scheme of insulator-film structure; **(d)** RCA cleaned surface without HF dipping. It causes formation of a thin SiO_2 chemical oxide layer at the surface. **(e)** NH_3 treatment (5×10^{-3} Pa, 400 °C) in the UHV chamber. A SiO_xN_y layer is formed at surface. **(f)** Oxide layer (HfO_2 ~15 nm thick) deposition by ALD for capacitor samples.

performed using HP4284A LCR meter and HP4145B semiconductor parameter analyzer, respectively. Silver paste was used as a backside contact.

3. Results and Discussion

3.1. Nitridation of the flash-heated Si(100)(2 × 1)+(1 × 2)

Fig. 2a presents a STM image of the Si(100)(2 × 1)+(1 × 2) surface cleaned in the UHV chamber by the flash heating manner. Two flash cycles were used, both of which raised the temperature of Si to 1200 °C for short time, couple of seconds, and then decreased back to 600 °C. The Si(100)(2 × 1)+(1 × 2) surface is so-called double-domain surface where dimer rows are along perpendicular directions at the neighboring terraces. The nitridation (NH_3 of 5 × 10^{-3} Pa for 30 min) of the clean surface was first tested by keeping Si at RT during the NH_3 exposure. Large-scale STM image after the RT nitridation (Fig. 2b) shows that the initial smooth terrace-step structure still remains. However, a local structure has changed due to the RT nitridation, as shown in Fig. 2c. Also, differential STS current-voltage curves (Fig. 2d) supports that nitrogen atoms have been incorporated into Si because a band gap of the surface has increased after the RT nitridation. It is worth noting that the band gap of the clean Si(100)(2 × 1)+(1 × 2) surface is about half of the bulk gap (1.1 eV) because of the surface dangling-bond induced levels. The N 1s emission, which is similar to that shown below after the 400 °C nitridation (Fig. 3), was also observed after the RT nitridation. This supports that nitrogen atoms are incorporated into the Si surface even in the RT nitridation without a plasma source.

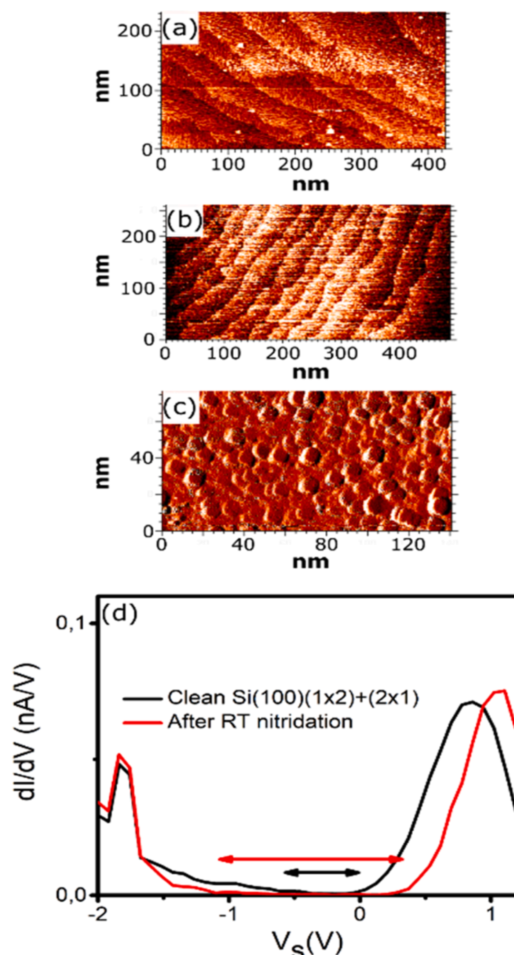

Fig. 2. **(a)** STM of starting Si(100)(2 × 1)+(1 × 2) surface which was flash cleaned. **(b)** STM after NH_3 exposure (5 × 10^{-3} Pa) at RT. **(c)** Zoomed-in STM after NH_3 exposure (5 × 10^{-3} Pa) at RT, showing formation of small islands. **(d)** Differential STS current-voltage curves to study the surface band gap: about 0.6 eV for the clean surface and 1.4 eV after the RT nitridation.

Fig. 3 summarizes effects of the nitridation of the Si(100)(2 × 1)+(1 × 2) surface at 400 °C. LEED from this surface in Fig. 3a shows still a clear (1 × 1) diffraction spots combined with weakened (2 ×)+(× 2) spots related to the surface reconstruction pattern after the 30 min nitridation at 400 °C. We note that LEED after the RT nitridation was similar to Fig. 3a. Large-scale STM image in Fig. 3b reveals the formation of small two-dimensional islands, while a zoomed-in STM image in the inset indicates that islands have still a local dimer-row structure, which is consistent with the LEED result showing weak (2 ×)+(× 2) spots. This indicates that the Si atoms occupy the topmost surface sites in the form of dimers although the nitrogen incorporation appears to cause a wavy height variation at the surface. The surface is crystalline at least to some extent after the nitridation according to the LEED and STM observations. The STS curve shows a surface band gap of 4.5 eV (Fig. 3c), which is near the Si_3N_4 gap, after the nitridation at 400 °C. The appearance of N 1s XPS signal (Fig. 3d) confirms the nitrogen incorporation into the sample. Large-scale STM image in Fig. 3e shows that the initial two-dimensional structure remains after the nitridation at 400 °C.

Comparison between the RT and 400 °C nitridations indicates similar LEED and XPS results for these surfaces, but the STS and local STM results are different. We did not observe the Si-dimer structure, similar to that in Fig. 3b, after the RT nitridation. Therefore, the weakened (2 ×)+(× 2) LEED spots after the RT nitridation can arise from a non-uniform surface, where a clean Si(100)(2 × 1)+(1 × 2) structure still remained locally.

Fig. 4 shows that the intensity at the high binding energy side of Si 2p increases as a function of the nitridation at 400 °C, which is due to the formation of Si-N bonding around 102 eV and Si-O-N bonding around 103 eV. Possible oxygen arises from contamination of the used gas or/and oxygen background of the chamber for instance. As discussed in the introduction, it is very difficult to avoid the oxygen incorporation into Si; thus a relevant question might be rather how to modify the properties of oxygen-containing surfaces. The presented results for the Si(100)(2 × 1)+(1 × 2) nitridation are in good agreement with the previous Si 2p results from nitrided insulator/SiGe interfaces [18]. The presence of dimer-row structure at the topmost surface suggests that nitrogen atoms lie at subsurface rather than on the topmost surface. Anyhow, the above results show that nitrogen atoms are incorporated into Si in the LT nitridation even at RT without a plasma source. Next, the nitridation is combined with the LT cleaning procedure of Si with the RCA wet chemistry, which is an industrially applicable cleaning procedure, to study effects of the nitridation on electrical properties.

3.2. Nitridation of RCA+HF dip cleaned Si(100)

First we present effects of the 400 °C nitridation on the capacitor properties, and below we compare to the RT nitridation effects. Fig. 5 shows electrical properties for the HfO_2/Si interfaces of which starting Si surfaces were cleaned by RCA+HF. The reference sample was directly transferred to ALD after the same RCA+HF treatment. The other sample was heated (at 400 °C for 30 min) and then nitrided (for 30 min) in the UHV chamber and after that, the sample was still transferred through air to ALD. Both capacitors (Fig.s 5a, 5b) present an inversion capacitance increase and saturation, which indicates the formation of negative fixed charge [e.g. 33-35]. It is worth noting that insulator-semiconductor interfaces typically include various types of electron levels (or traps) in the region of semiconductor band gap as well as outside of this gap at the interface and deeper in the insulator side. The electron levels which cause a permanent, fixed negative charge lie probably below the Si band gap region in the side of SiO_2 interface layer (i.e. acceptor type levels of SiO_2) [35]. Concerning the inversion capacitance, it is relevant that the inversion capacitance saturates with increasing the negative bias voltage. As O'Connor et al. [34] have instructively described, the

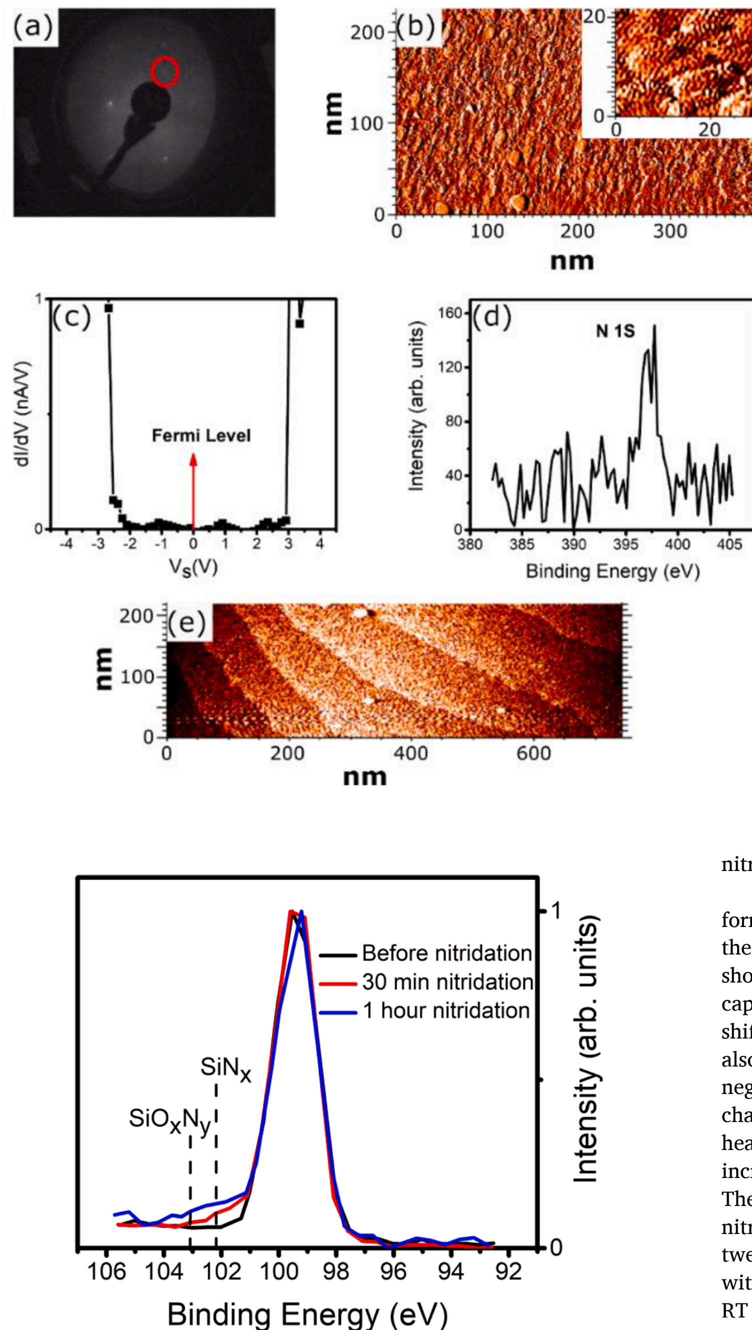

Fig. 3. Surface-science measurements after 30 min (at 400 °C) nitridation of Si(100)(2 × 1)+(1 × 2) surface cleaned by the flash heating up to 1200 °C. **(a)** LEED shows still a weak (2 × 1)+(1 × 2) pattern; one reconstruction spot is marked by red circle. **(b)** STM images; zoomed-in image shows local dimer rows. **(c)** STS indicates a surface band gap of around 4.5 eV. **(d)** XPS shows incorporation of nitrogen at the surface. **(e)** Large-scale STM shows that an initial two-dimensional terrace-step structure remains after 400 °C nitridation.

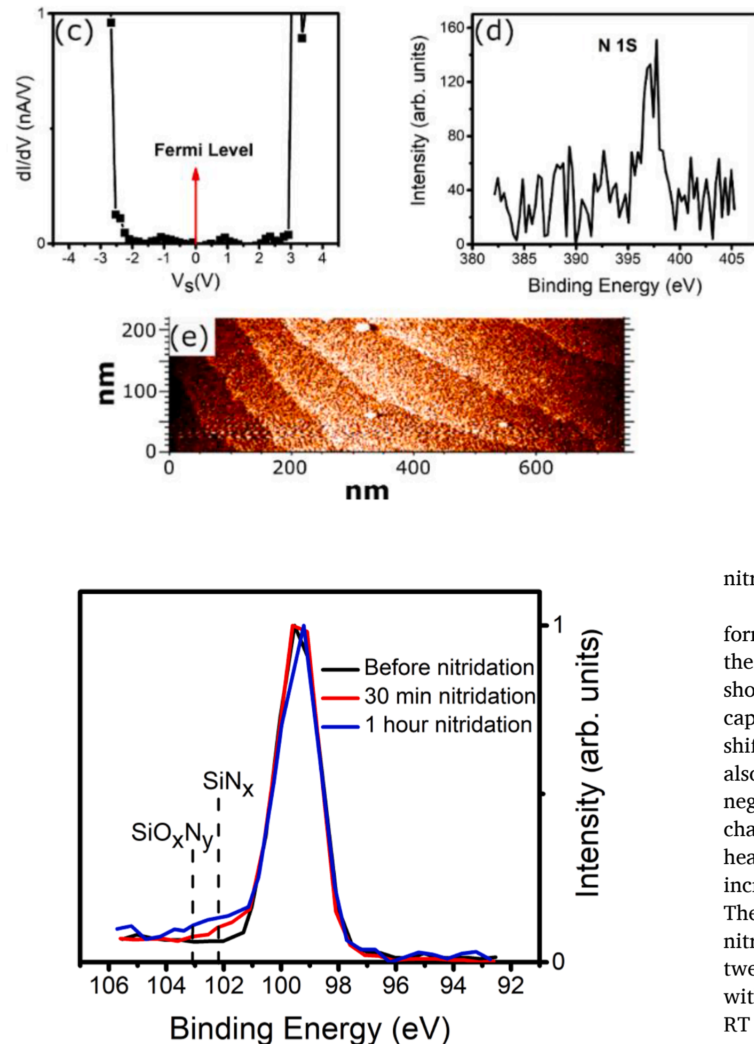

Fig. 4. XPS measurement of Si 2p before and after nitridation (at 400 °C) of Si (100)(2 × 1)+(1 × 2) surface cleaned by the flash heating. All spectra are normalized as to the peak intensity.

interface states do not contribute to the inversion capacitance saturation.

In contrast, the accumulation capacitance dispersion of the both samples with frequency is probably due to border traps [36–44] (i.e. gap levels deeper in SiO_2 or HfO_2 side) because the leakage current is low here. The nitridation increases the slope of the depletion-region capacitance step, as can be seen in Fig. 5. More quantitatively, a peak value of the differentiated C-V curves at the depletion region is 197 pF/V for the nitrided capacitor and 136 pF/V for the capacitor without the nitridation at 1 MHz [41,42]. These values are an average of 8 capacitors. The leakage current is also smaller for the capacitor with the nitridation. The leakage current density is 8.8 × 10^{-9} A/cm^2 at +2 V for the reference sample (Fig. 5d) and 6.5 × 10^{-9} A/cm^2 for the sample with the nitridation (Fig. 5e).

Then the nitridation of the RCA+HF cleaned Si surface was performed at RT before ALD. This sample was not annealed in UHV before the NH_3 exposure. The C-V curves and leakage of this capacitor are shown Fig. 5c and 5f respectively. For this sample, the inversion-capacitance did not increase and saturate, but the C step has clearly shifted to the positive voltage. Indeed, such a flat-band shift can arise also from the interface dipoles and/or trap levels, in addition to the fixed negative charge. Therefore, the C step can shift even if the fixed negative charge does not appear. However, after increasing the post metallization heating temperature near 500 °C (not shown), the inversion capacitance increased and saturated, but the depletion-region step also degraded. The peak slope of the C step (averaged over 8 capacitors) for the RT nitrided sample is 165 pF/V (after 400 °C post heating), which is between the above slopes for the 400 °C nitrided sample and the sample without the nitridation. Furthermore, the leakage current density of the RT nitrided capacitor is smaller at the positive voltage and larger at the negative voltage side (Fig. 5f). The reason for this remains unclear in this study although we speculate that the different leakage current behavior might arises from a charge storage effect via trap levels.

Thus, the simple LT nitridation method has potential to decrease the interface defect-level density at HfO_2/Si. This is consistent with the previous SiGe nitridation results [18], and also with the previous theoretical calculations that show a decrease in the Si-dangling-bond induced gap levels where N atoms replace the corresponding threefold bonded Si atoms at the interface [45–46].

3.3. *Nitridation of oxidized Si(100) prepared with the RCA recipe*

Because it is difficult to avoid the Si-surface oxidation during manufacturing Si devices, we have also studied the issue how the nitridation affects properties of the intentionally oxidized Si surface; namely RCA-treated wet-chemically oxidized Si. It is worth noting that very promising gate dielectric properties have been obtained by using a wet-chemical oxide interface [47].

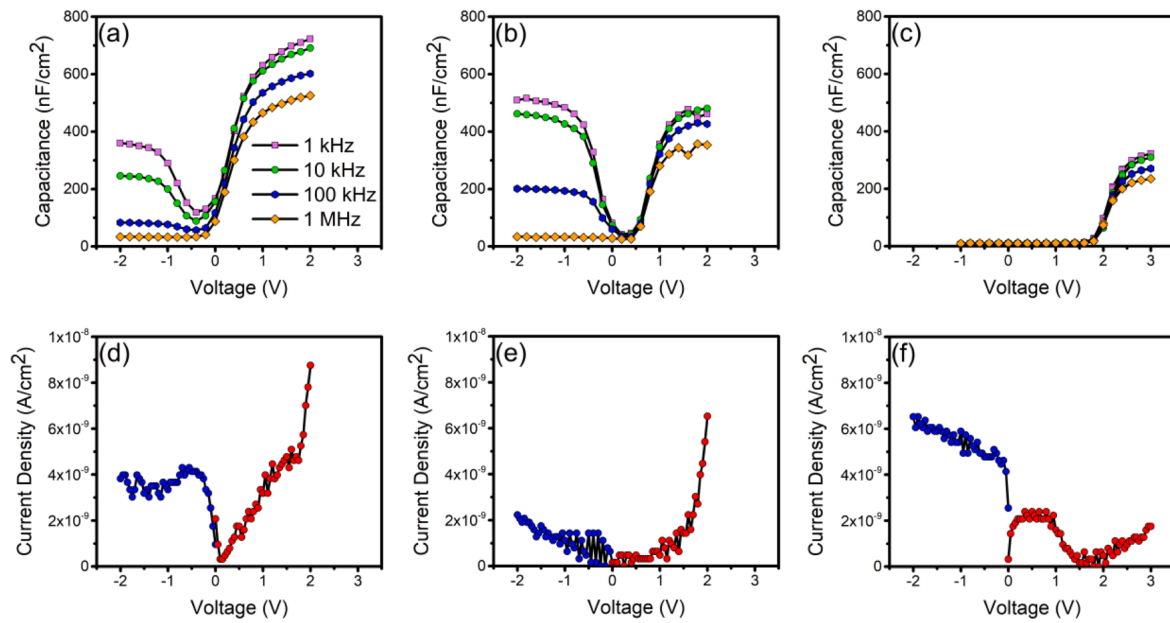

Fig. 5. Capacitor measurements for metal (Au/Cr) / HfO_2 / Si(100) cleaned by RCA + HF dip. **(a)** and **(d)** C-V curves and leakage for the sample without the nitrogen treatment before ALD. **(b)** and **(e)** C-V curves and leakage for the sample with the nitrogen treatment at 400 °C before ALD. **(c)** and **(f)** C-V curves and leakage for the sample with the nitrogen treatment at room temperature before ALD.

Fig. 6a shows the N 1s XPS spectrum from the SiO_2/Si sample prepared with the RCA recipe (Experimental section, without HF dip) after the nitridation. The curve fitting was performed using the Origin 2016 program. Shirley background shape and Voigt line shape were utilized to remove the inelastic background and to fit the spectrum. The measured N 1s line shape is asymmetric at high binding energy side, which is a clear indication of that the N 1s spectrum includes at least two components. Thus, two components were included in the fitting which provided one peak at 397.90 eV and another peak at 398.76 eV. These two components are consistent with the formation of two different bonding environments for N atoms: Si-N bond type (i.e. one N atom surrounded by silicon atoms) and Si-O-N bond type, as labeled in Fig. 6a [48–50]. Such a shift at high binding energy is attributed to the presence of oxygen close to the corresponding N atoms. For example, Lu et al. [48] have found that the SiO_xN_y/Si interface contains two N 1s components with 0.85 eV shift, which is close to our fitting result of 0.86 eV.

According to our XPS measurements, the O 1s emission (not shown here) did not change due to the nitridation indicating that the nitridation does not remove oxygen significantly from the SiO_2 film. However, the Si 2p spectra in Fig. 6a, 6b present an N-induced change in the Si bonding structure in the SiO_2 film or at the SiO_2/Si interface, supporting that the LT nitridation without a plasma source is potential to modify the properties of SiO_2/Si interface.

Fig. 7a represents the STM image from the wet-chemically oxidized Si(100) surface before the nitridation. This surface contains island or clusters. The inset LEED pattern in Fig. 7a shows no diffraction spots, indicating that the wet-chemically oxidized surface is mainly amorphous, as expected. Fig. 7b displays the STM from the oxidized surface after the nitridation. The morphology of the surface is similar to that before the nitridation, but STM suggests that the islands cover the surface more uniformly due to the nitridation. Fig. 7c shows the STS measurement before and after the nitridation (30 min and 60 min), respectively. Interestingly, a density of electron levels increases at 3 to 4 eV above the Fermi level due to the nitridation. This level can be intuitively understood as a donor-type level which forms if nitrogen replaces silicon in SiO_2. The electron level appears to be consistent also with the previous studies. Lee et al. [50] reported that the nitrogen-induced energy levels lie in the range of the Fermi level to the conduction band edge. These levels are dependent upon the local oxidation states around the nitrogen atom [48–50].

The C-V results for the capacitors with the wet-chemically oxidized Si interfaces (i.e. RCA without the final HF dip) in Fig. 8 indicate that the accumulation capacitance dispersion decreases when the nitridation was performed before ALD-HfO_2. This suggest that a density of border traps in SiO_2 decreases due to the nitridation. It is worth noting that the post heating after the metal contact were done in UHV chamber, which might enhance a vacancy formation in the oxide films. Furthermore, when the nitridation time is increased from 30 min to 1 hour, the inversion capacitance increase is suppressed, which indicates that the fixed negative charge in SiO_2 is decreased [33–35]. It is again worth noting that this permanent negative charge is most likely due to the filled acceptor levels in the side of SiO_2, which lie beneath the Si gap area in the energy scale. It is also possible that effect of the negative fixed charges is compensated by an opposite charge. Intuitively such scenario is consistent with the formation of donor-type gap levels above the Fermi level in SiO_2 (Fig. 7). In contrast, the movement of the depletion region capacitance step toward the positive voltage in Fig. 8 is most likely caused by the interface dipoles and/or by filling of other electron levels, different from the acceptor levels causing the negative fixed charge. Moreover, the nitridation increases the slope of the depletion-region capacitance step: The peak value of differentiated C-V curves at the depletion region is 120-160 pF/V for the nitrided capacitors and 100 pF/V for the capacitor without the nitridation for 1 MHz curves. Also the leakage current decreases because of the nitridation as illustrated in Fig. 8d.

Decreasing the equivalent oxide thickness (EOT) of capacitors, which provides an increased gate capacitance, has been a very important target in the transistor technology, and indeed a very low EOT of 0.65 nm has been recently obtained with a low leakage current [47]. EOT is defined as follows: $EOT = t_{SiO2} + t_{HfO2}/(\varepsilon_{HfO2}/\varepsilon_{SiO2})$, where t and ε are thickness and dielectric constant, respectively, for the interfacial SiO_2 layer and top HfO_2 film. If we use the measured thickness $t_{HfO2} = 15$ nm and the assumed values: $t_{SiO2} = 0.85$ nm, $\varepsilon_{SiO2} = 3.9$, and $\varepsilon_{HfO2} = 25.0$ from the literature [47,51], the above equation gives EOT = 3.2 nm for the reference sample with the RCA chemical oxide and without the nitridation. Future studies including detailed measurements of the oxide thickness and capacitance density as a function of the oxide thickness together with simulations are needed to clarify an effect of the presented

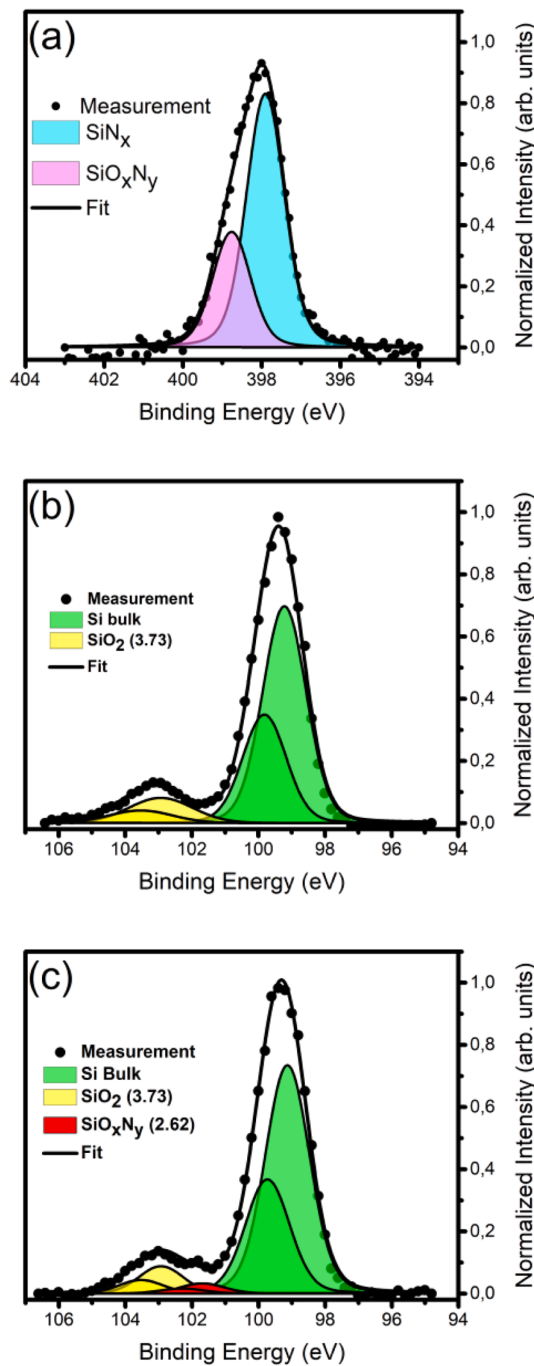

Fig. 6. (a) N 1s XPS measurement (ex situ) of Si(100) with the RCA chemical oxide after one hour nitridation. In-situ XPS measurements of Si 2p **(b)** before and **(c)** after the nitridation of the oxidized Si(100) surface, so called RCA chemical oxide (i.e. without HF-dip), respectively.

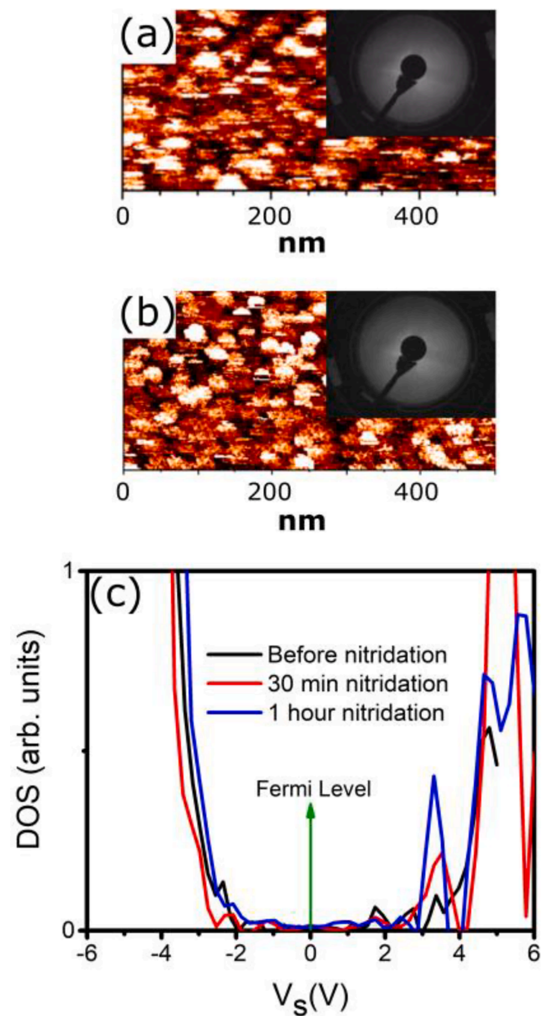

Fig. 7. Large scale STM images from Si(100) surface with RCA chemical oxide before **(a)** and after **(b)** the nitridation, respectively. The inset LEED patterns in (a) and (b) are from the corresponding surfaces, showing that the surfaces are mainly amorphous. **(c)** STS curves show the formation of N-induced levels 3-4 eV above the Fermi level (i.e. 0 V) after nitridation

nitridation on EOT. The previous studies have shown that the approach, where a proper SiO_2 wet-chemical oxide is incorporated before the HfO_2 deposition, is very potential to decrease EOT and to keep the oxide leakage current low enough [47,51].

4. Conclusion

We have investigated the effects of simple NH_3 nitridation of Si(100) surfaces in UHV chamber at low temperatures, RT or 400 °C, without a plasma source. The method enables the incorporation of N atoms into the different surfaces: clean Si and wet-chemically oxidized Si. The surface science characterization of clean Si after the nitridation supports that N atoms incorporate into subsurface sites. The LT nitridation of the wet-chemically oxidized SiO_2/Si surface hardly removes oxygen from the oxide but causes two different bonding environments for N atoms according to the N 1s signal analysis. The STS results reveal an increased density of the gap levels at 3 to 4 eV above the Fermi level. In comparison to the two different RCA-treated reference interfaces, HfO_2/Si and HfO_2/SiO_x/Si, the nitridation has been indirectly found to decrease the interface D_{it} on the basis of the capacitor measurements. Thus, the LT-UHV nitridation is potential to be incorporated into an arsenal of the passivation methods of Si device interfaces.

CRediT authorship contribution statement

Masoud Ebrahimzadeh: experiments, measurements, data analysis, writing. **Juha-Pekka Lehtiö**: experiments, data analysis, writing. **Marko Punkkinen**: writing. **Risto Punkkinen**: experiments, writing. **Mikko Miettinen**: experiments, writing. **Zahra Sadat Jahanshah Rad**: writing. **Mikhail Kuzmin**: analysis, writing. **Pekka Laukkanen**: experiments, data analysis, writing. **Kalevi Kokko**: analysis, writing.

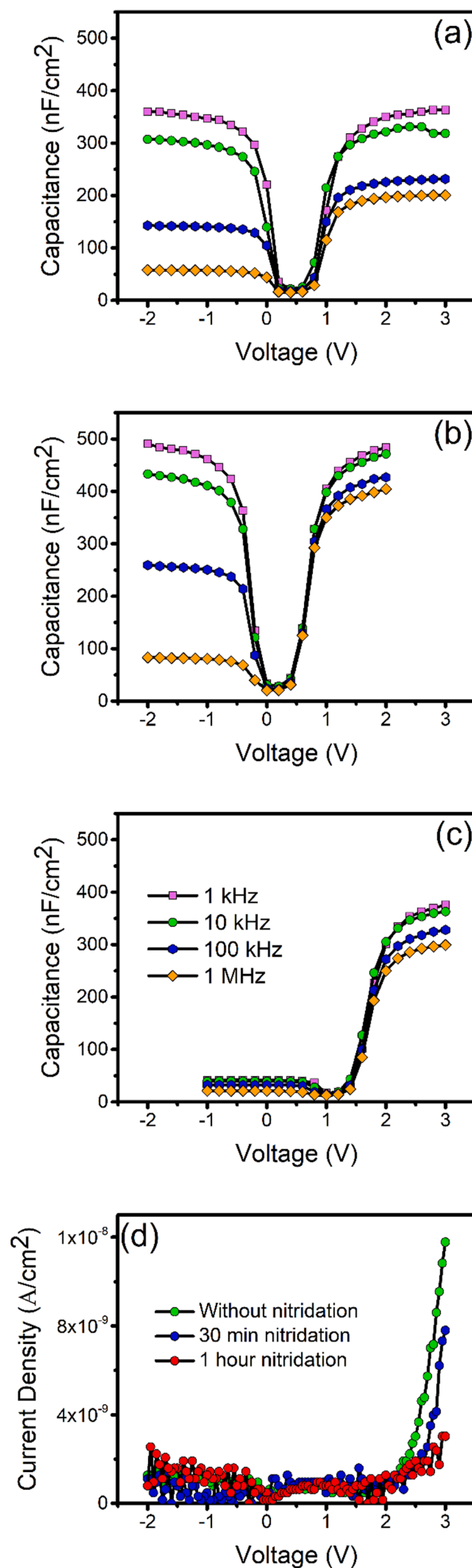

Fig. 8. C-V properties comparison for metal (Ag/Cr)/ HfO_2/ Si(100) stack with the RCA chemical oxide (without HF dip) **(a)** without UHV nitrogen treatment **(b)** 30 min UHV nitrogen treatment, and **(c)** 1 hour UHV nitrogen treatment **(d)** Leakage current measurements for metal (Ag/Cr) / HfO2 / Si(100) stack with RCA chemical oxide interfaces.

Declaration of Competing Interest

We do not have any conflicts to disclose, concerning our submission effects of ammonia (NH3) nitridation of Si(100) surfaces in ultrahigh vacuum at 400 °C.

Data Availability

Data will be made available on request.

Acknowledgements

This work has been supported by the University of Turku Graduate School (UTUGS), the Academy of Finland (via the project # 338973).

References

[1] Y.J. Chabal, Fundamental Aspects of Silicon Oxidation, Springer, Berlin, 2001 first ed.

[2] A.A. Demkov, A. Navrotsky, Materials Fundamentals of Gate Dielectrics, Springer, Dordrecht, 2005 first ed.

[3] F.H.P.M. Habraken, A.E.T. Kuiper, Oxidation of silicon (oxy)nitride and nitridation of silicon dioxide: Manifestations of the same chemical reaction system? Thin Solid Films 193-194 (1990) 665–674, https://doi.org/10.1016/0040-6090(90)90217-2.

[4] G.D. Wilk, R.M. Wallace, J.M. Anthony, High-K gate dielectrics: Current status and materials properties considerations, J. Appl. Phys. 89 (2001) 5243–5275, https://doi.org/10.1063/1.1361065.

[5] P. D. Kirsch, M. A. Quevedo-Lopez, S. A. Krishnan, C. Krug, H. AlShareef, C. S. Park, R. Harris, N. Moumen, A. Neugroschel, G. Bersuker, B. H. Lee, J. G. Wang, G. Pant, B. E. Gnade, M. J. Kim, R. M. Wallace, J. S. Jur, D. J. Lichtenwalner, A. I. Kingon, R. Jammy, Band Edge n-MOSFETs with High-k/Metal Gate Stacks Scaled to EOT=0.9nm with Excellent Carrier Mobility and High Temperature Stability, 2006 International Electron Devices Meeting, San Francisco, CA, USA, December 11-13, New York, IEEE (2006), pp.1-4, 10.1109/IEDM.2006.346862.

[6] P.K. Hurley, K. Cherkaoui, A.W. Groenland, Electrically Active Interface Defects in (100) Si/SiO_x/HfO_2/TiN System: Origin, Instabilities, and Passivation, ECS Trans 3 (2006) 97, https://doi.org/10.1149/1.2355702.

[7] S. Datta, S. Dutta, B. Grisafe, J. Smith, S. Srinivasa, H. Ye, Back-end-of-line compatible transistors for monolithic 3-D integration, IEEE Micro 39 (6) (2019) 8–15, https://doi.org/10.1109/MM.2019.2942978.

[8] L. Brunet, C. Fenouillet-Beranger, P. Batude, S. Beaurepaire, F. Ponthenier, N. Rambal, V. Mazzocchi, J.-B. Pin, P. Acosta-Alba, S. Kerdiles, P. Besson, H. Fontaine, T. Lardin, F. Fournel, V. Larrey, F. Mazen, V. Balan, C. Morales, C. Guerin, V. Jousseaume, X. Federspiel, D. Ney, X. Garros, A. Roman, D. Scevola, P. Perreau, F. Kouemeni-Tchouake, L. Arnaud, C. Scibetta, S. Chevalliez, F. Aussenac, J. Aubin, S. Reboh, F. Andrieu, S. Maitrejean, M. Vinet, in: Breakthroughs in 3D Sequential Technology, 2018 IEEE International Electron Devices Meeting, San Francisco, CA, USA, December 1-5, 2018, IEEE, New York, 2018, p. 7.2, https://doi.org/10.1109/IEDM.2018.8614653, 1-7.2.4.

[9] Z.J. Rad, J.P. Lehtiö, I. Mack, K. Rosta, K. Chen, V. Vähänissi, M. Punkkinen, R. Punkkinen, H.P. Hedman, A. Pavlov, M. Kuzmin, H. Savin, P. Laukkanen, K. Kokko, Decreasing Interface Defect Densities via Silicon Oxide Passivation at Temperatures Below 450°C, ACS Appl. Mater. Interfaces 12 (2020) 46933, https://doi.org/10.1021/acsami.0c12636. -4694.

[10] T. Seo, H. Park, G. Jeon, J. Yun, S. Park, S. Seong, Y. Chung, Low-Temperature Fabrication (≤ 150°C) of High-Quality Sputtered Silicon Oxide Thin Film with Hydrogen Plasma Treatment, ACS Appl. Electron. Mater. 2 (2020) 3320–3326, https://doi.org/10.1021/acsaelm.0c00631.

[11] P.K. Hurley, B.J. O'Sullivan, V.V. Afanas'ev, A. Stesmans, Interface States and P_b Defects at the Si (100)/HfO_2 Interface, ECS Solid State Lett 8 (2004) G44, https://doi.org/10.1063/1.3527909.

[12] J. Robertson, R.M. Wallace, High-K materials and metal gates for CMOS applications, Mater. Sci. Eng. R Rep. 88 (2015) 1–41, https://doi.org/10.1016/j.mser.2014.11.001.

[13] G. Dingemans, W.M.M. Kessels, Status and prospects of Al_2O_3-based surface passivation schemes for silicon solar cells, J. Vac. Sci. Technol. A 30 (2012), 040802, https://doi.org/10.1116/1.4728205.

[14] T.G. Allen, J. Bullock, X. Yang, A. Javey, S. De Wolf, Passivating contacts for crystalline silicon solar cells, Nat. Energy 4 (2019) 914–928, https://doi.org/10.1038/s41560-019-0463-6.

[15] S. Chaoudhary, A. Dewasi, S. Ghosh, R.J. Choudhary, D.M. Phase, T. Ganguli, V. Rastogi, R.N. Pereira, A. Sinopoli, B. Aïssa, A. Mitra, X-ray photoelectron spectroscopy and spectroscopic ellipsometry analysis of the p-NiO/n-Si heterostructure system grown by pulsed laser deposition, Thin Solid Films 743 (2021) 13907, https://doi.org/10.1016/j.tsf.2021.139077.

[16] A. Uzuma, I. Kanmaz, Passivation properties of HfO_2-SiO_2 mixed metal oxide thin films with low reflectivity on silicon substrates for semiconductor devices, Thin Solid Films 738 (2021), 138965, https://doi.org/10.1016/j.tsf.2021.138965.

[17] A. Rawat, K.K. Roluahpuia, S. Rowtu, V. Belwanshi, A. Laha, S. Mahapatra, U. Ganguly, Radio frequency power controlled crystal phase transition from

monoclinic to cubic, Thin Solid Films 742 (2022), 139047, https://doi.org/10.1016/j.tsf.2021.139047.
[18] K. Sardashti, K-T Hu, K. Tang, Sh. Madisetti, P. McIntyre, S. Oktyabrsky, S. Siddiqui, B. Sahu, N. Yoshida, J. Kachian, L. Dong, B. Fruhberger, A.C. Kummel, Nitride passivation of the interface between high-k dielectrics and SiGe, Appl. Phys. Lett. 108 (2016), 011604, https://doi.org/10.1063/1.4939460.
[19] F. Tian, A.V. Teplyakov, Silicon surface functionalization targeting Si-N linkages, Langmuir 29 (2013) 13–28, https://doi.org/10.1021/la303505s.
[20] J.W. Kim, H.W. Yeom, K.J. Kong, B.D. Yu, D.Y. Ahn, Y.D. Chung, C.N. Whang, H. Yi, Y.H. Ha, D.W. Moon, Spontaneous N incorporation onto a Si (100) surface, Phys. Rev. Lett. 90 (2003) 106101–106105, https://doi.org/10.1103/PhysRevLett.90.106101.
[21] X.S. Wang, G. Zhai, J. Yang, L. Wang, Y. Hu, Z. Li, J.C. Tang, X. Wang, K.K. Fung, N. Cue, Nitridation of Si (111), Surf. Sci. 494 (2001) 83–94, https://doi.org/10.1016/S0039-6028(01)01409-1.
[22] T.L. Petrenko, V.P. Bryksa, I.V. Dyka, V.P. Kladko, A.E. Belyaev, A.V. Kuchuk, Microscopic mechanisms of Si (111) surface nitridation and energetics of Si_3N_4/Si (111) interface, Appl. Surf. Sci. 483 (2019) 302–312, https://doi.org/10.1016/j.apsusc.2019.03.239.
[23] Y. Oshima, Y. Sun, D. Kuzum, T. Sugawara, K.C. Saraswat, P. Pianetta, P. C. McIntyre, Chemical bonding, interfaces, and defects in hafnium oxide/germanium oxynitride gate stacks on Ge(100), J. Electrochem. Soc. 155 (2008) G304–G309, https://doi.org/10.1149/1.2995832.
[24] E.C. Carr, R.A. Buhrman, Role of interfacial nitrogen in improving thin silicon oxides grown in N_2O, Appl. Phys. Lett. 63 (1993) 54–56, https://doi.org/10.1063/1.109749.
[25] Z.Q. Yao, H.B. Harrison, S. Dimitrijev, D. Sweatman, Y.T. Yeow, High quality ultrathin dielectric films grown on silicon in a nitric oxide ambient, Appl. Phys. Let. 64 (1994) 3584–3586, https://doi.org/10.1063/1.111205.
[26] V. Bhatt, S. Chandra, Silicon nitride films deposited by RF sputtering for microstructure fabrication in MEMS, J. Electron. Mater. 38 (2009) 1979–1989, https://doi.org/10.1007/s11664-009-0846-8.
[27] K. Sekine, Y. Saito, M. Hirayama, T. Ohmi, Highly robust ultrathin silicon nitride films grown at low-temperature by microwave-excitation high-density plasma for giga scale integration, IEEE Trans. Electron Devices. 47 (7) (2000) 1370–1374, https://doi.org/10.1109/16.848279.
[28] D.K. Rai, C.S. Solanki, B.R. Kavaipatti, Growth of silicon nitride by nitridation of amorphous silicon at low temperature in hot-wire CVD, Mater. Sci. Semicond. Process. 67 (2017) 46–54, https://doi.org/10.1016/j.mssp.2017.05.015.
[29] A. Ikeda, M.A. Elnaby, R. Hattori, Y. Kuroki, Effect of nitrogen plasma conditions on electrical properties of silicon oxynitrided thin films for flash memory applications, Thin Solid Films 386 (2001) 111–116, https://doi.org/10.1016/S0040-6090(00)01888-5.
[30] J.P. Campbell, P.M. Lenahan, A.T. Krishnan, S. Krishnan, Location, Structure, and Density of States of NBTI-Induced Defects in Plasma Nitrided pMOSFETs, in: 2007 IEEE International Reliability Physics Symposium Proceedings. 45th Annual, Phoenix, AZ, USA, April 15-19, IEEE, New York, 2007, pp. 503–510, https://doi.org/10.1109/RELPHY.2007.369942.
[31] M. Sadiq, S. Ahmad, M. Shafiq, M. Zakaullah, Nitrogen ion implantation of silicon in dense plasma focus, Nucl. Instrum. Methods Phys. Res. B: Beam Interact. Mater. At. 252 (2006) 219–224, https://doi.org/10.1016/j.nimb.2006.08.020.
[32] H.J. Kim, D.H. Kim, W. Lee, Y.H. Roh, Gate leakage properties on n-MOSFET with plasma oxidized and nitride, in: 2009 International Semiconductor Device Research Symposium, College Park, MD, USA, December 9-11, IEEE, New York, 2009, pp. 182–185, https://doi.org/10.1109/ISDRS.2009.5378201.
[33] J.P. Lehtiö, Z.J. Rad, S. Granroth, M. Yasir, M. Punkkinen, R. Punkkinen, H. P. Hedman, J.P. Rueff, I.T. Rauha, H. Savin, P. Laukkanen, K. Kokko, Observation of Si 2p Core-Level Shift in Si/High-κ Dielectric Interfaces Containing a Negative Charge, Adv. Electron. Mater. 7 (2021), 2100034, https://doi.org/10.1002/aelm.202100034.
[34] É. O'Connor, K. Cherkaoui, S. Monaghan, D. O'Connell, I. Povey, P. Casey, S. B. Newcomb, Y.Y. Gomeniuk, G. Provenzano, F. Crupi, G. Hughes, P.K. Hurley, Observation of peripheral charge induced low frequency capacitance-voltage behaviour in metal-oxide-semiconductor capacitors on Si and GaAs substrates, J. Appl. Phys. 111 (2012), 124104, https://doi.org/10.1063/1.4729331.
[35] D. König, D. Hiller, S. Gutsch, M. Zacharias, S. Smith, Modulation doping of silicon using aluminium-induced acceptor states in silicon dioxide, Sci. Rep. 7 (2017) 1–8, https://doi.org/10.1038/srep46703.
[36] S. Stemmer, V. Chobpattana, S. Rajan, Frequency dispersion in III-V metal-oxide-semiconductor capacitors, Appl. Phys. Lett. 100 (2012), 233510, https://doi.org/10.1063/1.4724330.
[37] G. Brammertz, H.C. Lin, K. Martens, D. Mercier, C. Merckling, J. Penaud, C. Adelmann, S. Sioncke, W.E. Wang, M. Caymax, M. Meuris, M. Heyns, Capacitance–voltage characterization of GaAs-oxide interfaces, J. Electrochem. Soc. 155 (2008) H945, https://doi.org/10.1149/1.2988045.
[38] I. Krylov, D. Ritter, M. Eizenberg, The physical origin of dispersion in accumulation in InGaAs based metal oxide semiconductor gate stacks, J. Appl. Phys. 117 (2015), 174501, https://doi.org/10.1063/1.4919600.
[39] J. Lin, S. Monaghan, K. Cherkaoui, I. Povey, É. O'Connor, B. Sheehan, P. Hurley, A study of capacitance–voltage hysteresis in the HfO_2/InGaAs metal-oxide-semiconductor system, Microelectron. Eng. 147 (2015) 273–276, https://doi.org/10.1016/j.mee.2015.04.108.
[40] T.C. Chang, S.T. Yan, P.T. Liu, C.W. Chen, Y.C. Wu, S.M. Sze, Study on SONOS nonvolatile memory technology using high-density plasma CVD silicon nitride, ECS Solid State Lett 7 (2004) G113, https://doi.org/10.1149/1.1695537.
[41] R. Engel-Herbert, Y. Hwang, S. Stemmer, Comparison of methods to quantify interface trap densities at dielectric/III-V semiconductor interfaces, J. Appl. Phys. 108 (2010), 124101, https://doi.org/10.1063/1.3520431.
[42] C.W. Cheng, G. Apostolopoulos, E.A. Fitzgerald, The effect of interface processing on the distribution of interfacial defect states and the CV characteristics of III-V metal-oxide-semiconductor field effect transistors, J. Appl. Phys. 109 (2011), 023714, https://doi.org/10.1063/1.3537915.
[43] Y.C. Byun, S. Choi, Y. An, P.C. McIntyre, H. Kim, Tailoring the interface quality between HfO_2 and GaAs via in situ ZnO passivation using atomic layer deposition, ACS Appl. Mater. Interfaces 6 (2014) 10482–10488, https://doi.org/10.1021/am502048d.
[44] K. Martens, C.O. Chui, G. Brammertz, B. De Jaeger, D. Kuzum, M. Meuris, M. Heyns, T. Krishnamohan, K. Saraswat, H.E. Maes, G. Groeseneken, On the correct extraction of interface trap density of MOS devices with high-mobility semiconductor substrates, IEEE Transactions on Electron Devices 55 (2) (2008) 547–556, https://doi.org/10.1109/TED.2007.912365.
[45] P. Gupta, M. Soni, S.K. Sharma, Alternate lanthanum oxide/silicon oxynitride-based gate stack performance enhancement due to ultrathin oxynitride interfacial layer for CMOS applications, J. Mater. Sci.: Mater. Electron. 31 (2020) 1986–1995, https://doi.org/10.1007/s10854-019-02718-7.
[46] K. Taniguchi, M. Tanaka, C. Hamaguchi, K. Imai, Density relaxation of silicon dioxide on (100) silicon during thermal annealing, J. Appl. Phys. 67 (1990) 2195–2198, https://doi.org/10.1063/1.345563.
[47] S.S. Cheema, N. Shanker, L.C. Wang, C.H. Hsu, S.L. Hsu, Y.H. Liao, M.S. Jose, J. Gomez, W. Chakraborty, W. Li, J.H. Bae, S.K. Volkman, D. Kwon, Y. Rho, G. Pinelli, R. Rastogi, D. Pipitone, C. Stull, M. Cook, B. Tyrrell, V.A. Stoica, Z. Zhang, J.W. Freeland, C.J. Tassone, A. Mehta, G. Saheli, D. Thompson, D.I. Suh, W.T. Koo, K.J. Nam, D.J. Jung, W.B. Song, C.H. Lin, S. Nam, J. Heo, N. Parihar, C. P. Grigoropoulos, P. Shafer, P. Fay, R. Ramesh, S. Mahapatra, J. Ciston, S. Datta, M. Mohamed, C. Hu, S. Salahuddin, Ultrathin ferroic HfO_2-ZrO_2 superlattice gate stack for advanced transistors, Nature 604 (7904) (2022) 65–71, https://doi.org/10.1038/s41586-022-04425-6.
[48] Z.H. Lu, S.P. Tay, R. Cao, P. Pianetta, The effect of rapid thermal N_2O nitridation on the oxide/Si (100) interface structure, Appl. Phys. Lett. 67 (1995) 2836–2838, https://doi.org/10.1063/1.114801.
[49] F.J. Himpsel, F.R. McFeely, A. Taleb-Ibrahimi, J.A. Yarmoff, G. Hollinger, Microscopic structure of the SiO_2/Si interface, Phys. Rev. *B* 38 (1988) 6084, https://doi.org/10.1103/PhysRevB.38.6084.
[50] E.C. Lee, Nitrogen-induced interface defects in Si oxynitride, Phys. Rev. *B* 77 (2008), 104108, https://doi.org/10.1103/PhysRevB.77.104108.
[51] S. Li, L. Han, Z. Chen, The Interfacial Quality of HfO_2 on Silicon with DifferentThicknesses of the Chemical Oxide Interfacial Layer, J. Electrochem. Soc. 157 (2010) G221, https://doi.org/10.1149/1.3483789.